Large Deflection Analysis of Elastic-Plastic Shells Using Numerical Integration

J. C. GERDEEN*
Michigan Technological University, Houghton, Mich.
F. A. SIMONEN† AND D. T. HUNTER‡
Battelle Memorial Institute, Columbus, Ohio

Nonlinear problems are treated which involve geometrical nonlinearities occurring because of geometry changes and material nonlinearities resulting from plastic strains. Accurate numerical analysis is achieved by use of a computer program based on nonlinear shell theory and a multisegment method of numerical integration. Shell stiffnesses are evaluated numerically for the von Mises yield criterion and in closed form for the Tresca criterion. Collapse behavior of pressure vessel heads as predicted by linear and nonlinear analyses are compared. The pressure deflection response of a convoluted stainless steel bellows is calculated, and is seen to compare favorably with experimental results.

Nomenclature

h = shell thickness
M_ϕ, M_θ = bending moment resultants in the meridional and circumferential directions
N_ϕ, N_θ = membrane resultant forces in the meridional and circumferential directions
p_ϕ, p = pressure or body force loading in meridional and normal directions
Q_ϕ = shear resultant
r = radial distance from axis of revolution
R_ϕ = meridional radius of curvature
s = distance measured along meridian of shell
u_ϕ = displacement in meridional direction
w = displacement normal to shell
β_ϕ = rotation of normal to shell
$\epsilon_\phi, \epsilon_\theta$ = midsurface membrane strains in meridional and circumferential directions
θ = angle measured in circumferential direction
$\kappa_\phi, \kappa_\theta$ = change in curvature in meridional and circumferential directions
ϕ = angle between normal to shell and axis of revolution

Introduction

THIS paper is concerned with the accurate numerical analysis of elastic-plastic shells of revolution by use of the multisegment method of numerical integration.[1] Marcal and Pilgrim[2] have presented a numerical integration method of elastic-plastic analysis, but it was limited to small deflections. In more recent work, the finite element method has been applied to large deflection analysis of elastic-plastic shells by Marcal[3-5] and Popov and Yaghmai.[6,7] Both Marcal and Yaghmai used the curved shell element of Khojasteh-Bakht.[8] In Ref. 5, Marcal also uses a triangular plate element known as the DeVeubeke element. Both Marcal and Yaghmai linearized the problem over small load increments. The geometry was then updated after each load increment. This approximate method seems to converge if the increments are sufficiently small.

Numerical integration solutions to large deflection elastic-plastic shell problems have not appeared in the literature to the authors' knowledge. Numerical integration enables a direct solution to the nonlinear differential equations, and accuracy can be automatically controlled during the integration by predictor-corrector methods of adjusting the step size. Also, the multisegment method[1] provides a means of accurate solution over long integration paths, with an iteration procedure being employed to satisfy the boundary conditions. A fundamental difference between geometrically linear and geometrically nonlinear elastic plastic problems should be noted. For the former, the equilibrium equations can be formulated in terms of the increments in stress resultants, but for the latter this is not possible. Geometry changes influence the equilibrium equations, and both the deformed geometry and the total stress resultants must be considered.

Large deflections of shells are accompanied by plastic strains. Therefore, an accurate analysis requires that partial yielding through the shell thickness be accounted for. This is done in the present work by deriving closed-form expressions for the elastic-plastic shell stiffnesses for incremental loading according to the Tresca yield criterion.[9] For the von Mises criterion, however, closed-form expressions cannot be found and the stiffnesses have to be found by integration over the shell thickness as in Ref. 2. The latter require storage of stresses at a large number of points through the thickness of the shell at each station along the shell meridian. When applicable, the Tresca stiffness derivations presented in this paper require data at four points at most through the thickness, and thereby reduce the computer storage requirements.

Governing Shell Equations

The governing shell equations include six differential equations for the fundamental variables: $w, Q_\phi, u_\phi, N_\phi, \beta_\phi$, and M_ϕ. These result from the three equilibrium equations and three of the strain displacement relations for a shell of revolution (neglecting shear deformation). These equations appropriate to Sander's Theory for small strains but moderately large rotations[10,11] are as follows:

$$w_{,s} = u_\phi/R_\phi - \beta_\phi \tag{1}$$

Received July 23, 1970; revision received February 9, 1971. The numerical results for the torispherical head were generated at Battelle's Columbus Laboratories under sponsorship of the Pressure Vessel Research Committee of the Welding Research Council.

* Associate Professor, Department of Mechanical Engineering and Engineering Mechanics. Member AIAA.

† Research Engineer, Advanced Solid Mechanics Division. Member AIAA.

‡ Research Engineer, Advanced Solid Mechanics Division, now Assistant Professor, Mechanical and Aerospace Engineering Department, Louisiana State University, Baton Rouge, La. Associate Member AIAA.

$$Q_{\phi,s} = N_\theta(\sin\phi + \beta_\phi \cos\phi)/r - Q_\phi(\beta_\phi/R_\phi + \cos\phi/r) + N_\phi[\beta_{\phi,s} + (1 + \beta_\phi)/R_\phi] - p \quad (2)$$

$$u_{\phi,s} = \epsilon_\phi - w/R_\phi - \beta_\phi{}^2/2 \quad (3)$$

$$N_{\phi,s} = (N_\theta - N_\phi)\cos\phi/r + (\beta_\phi N_\phi - Q_\phi)/R_\phi - p_\phi \quad (4)$$

$$\beta_{\phi,s} = \kappa_\phi \quad (5)$$

$$M_{\phi,s} = (M_\theta - M_\phi)\cos\phi/r + Q_\phi \quad (6)$$

The fundamental variables are ordered as in Eqs. (1–6). These quantities appear in the natural boundary conditions and only one or the other of w and Q_ϕ, or u_ϕ and N_ϕ, or β_ϕ and M_ϕ can be specified at a boundary. Both w and Q_ϕ, for example, cannot be specified. However, linear combinations of w and Q_ϕ can be specified (e.g., at an elastically restrained edge). Sander's Theory is used here, but any nonlinear theory could be used. Reissner's nonlinear shell theory[12] is equally applicable. Equations (1–6) apply for large deflections of any shell with arbitrary material constitutive laws. A constitutive law relates the auxiliary variables $N_\theta, M_\theta, \epsilon_\phi$, and κ_ϕ appearing in Eqs. (1–6) to the fundamental variables. An incremental form of the stress-strain relations is assumed here and will be shown to have the following form:

$$\Delta N_\phi = C_{11}\Delta\epsilon_\phi + C_{12}\Delta\epsilon_\theta + K_{11}\Delta\kappa_\phi + K_{12}\Delta\kappa_\theta \quad (7)$$

$$\Delta N_\theta = C_{12}\Delta\epsilon_\phi + C_{22}\Delta\epsilon_\theta + K_{12}\Delta\kappa_\phi + K_{22}\Delta\kappa_\theta \quad (8)$$

$$\Delta M_\phi = D_{11}\Delta\kappa_\phi + D_{12}\Delta\kappa_\theta + K_{11}\Delta\epsilon_\phi + K_{12}\Delta\epsilon_\theta \quad (9)$$

$$\Delta M_\theta = D_{12}\Delta\kappa_\phi + D_{22}\Delta\kappa_\theta + K_{12}\Delta\epsilon_\phi + K_{22}\Delta\epsilon_\theta \quad (10)$$

where $\Delta N_\phi = N_\phi - N_{\phi r}$, $N_{\phi r}$ = the residual N_ϕ from the previous loading step, etc. This form of the constitutive relations for an elastic-plastic shell of isotropic material resembles that for a layered orthotropic elastic shell.[13]

The auxiliary variables needed in Eqs. (1–6) can be calculated in the following order:

$$\epsilon_\theta = (u_\phi \cos\phi + w \sin\phi)/r, \quad \kappa_\theta = \beta_\phi \cos\phi/r \quad (11a)$$

$$\Delta\epsilon_\theta = \epsilon_\theta - \epsilon_{\theta r}, \quad \Delta\kappa_\theta = \kappa_\theta - \kappa_{\theta r} \quad (11b)$$

$$\Delta N_\phi = N_\phi - N_{\phi r}, \quad \Delta M_\phi = M_\phi - M_{\phi r} \quad (11c)$$

$$A_1 = C_{11}D_{11} - K_{11}{}^2 \quad (11d)$$

$$\Delta\epsilon_\phi = [(\Delta N_\phi - C_{12}\Delta\epsilon_\theta - K_{12}\Delta\kappa_\theta)D_{11} - (\Delta M_\phi - K_{12}\Delta\epsilon_\theta - D_{12}\Delta\kappa_\theta)K_{11}]/A_1 \quad (11e)$$

$$\Delta\kappa_\phi = [(\Delta M_\phi - K_{12}\Delta\epsilon_\theta - D_{12}\Delta\kappa_\theta)C_{11} - (\Delta N_\phi - C_{12}\Delta\epsilon_\theta - K_{12}\Delta\kappa_\theta)K_{11}]/A_1 \quad (11f)$$

$$\epsilon_\phi = \epsilon_{\phi r} + \Delta\epsilon_\phi, \quad \kappa_\phi = \kappa_{\phi r} + \Delta\kappa_\phi \quad (11g)$$

$$\Delta N_\theta = \text{Eq. (8)}, \quad \Delta M_\theta = \text{Eq. (10)} \quad (11h)$$

$$N_\theta = N_{\theta r} + \Delta N_\theta, \quad M_\theta = M_{\theta r} + \Delta M_\theta \quad (11i)$$

Elastic-Plastic Shell Stiffnesses

The stiffnesses C_{ij}, K_{ij}, and D_{ij} are defined as follows:

$$C_{ij} = \int_{-h/2}^{h/2} E_{ij}dz, \quad K_{ij} = \int_{-h/2}^{h/2} E_{ij}z dz, \quad D_{ij} = \int_{-h/2}^{h/2} E_{ij}z^2 dz \quad (12)$$

$$\begin{bmatrix} d\sigma_1 \\ d\sigma_2 \\ d\bar{\epsilon}_p \end{bmatrix} = \begin{bmatrix} E_{11} & E_{12} \\ E_{12} & E_{22} \\ E_{13} & E_{23} \end{bmatrix} \cdot \begin{bmatrix} d\epsilon_1 \\ d\epsilon_2 \end{bmatrix} \quad (13)$$

The E_{ij} are the elastic-plastic moduli for a plane stress state. They differ depending upon the yield criterion used. The stresses σ_1 and σ_2 and the strains ϵ_1 and ϵ_2 correspond to the directions of ϕ and θ, respectively, for a shell of revolution.

The shell stiffnesses defined in Eq. (12) result from the definitions of the stress resultants (in incremental form):

$$dN_\phi = \int_{-h/2}^{h/2} d\sigma_1 dz, \quad dN_\theta = \int_{-h/2}^{h/2} d\sigma_2 dz$$
$$dM_\phi = \int_{-h/2}^{h/2} z d\sigma_1 dz, \quad dM_\theta = \int_{-h/2}^{h/2} z d\sigma_2 dz \quad (14)$$

The Kirchhoff hypothesis of a linear strain distribution through the thickness is assumed, i.e.,

$$d\epsilon_1 = d\epsilon_\phi + d\kappa_\phi \cdot z, \quad d\epsilon_2 = d\epsilon_\theta + d\kappa_\theta \cdot z \quad (15)$$

Substitution of Eq. (15) into Eq. (13) and Eq. (13) into Eq. (14) gives the results in Eq. (12) to be used in Eqs. (7–10). Equations (7–10) have been written in terms of finite (Δ) increments, whereas Eq. (13) is strictly a differential law. This is only exact when the E_{ij} are constant, otherwise it is an approximation depending upon the size of the increments taken. It happens to be exact for the Tresca criterion with linear strain hardening.

The E_{ij} are determined using the potential flow law for the plastic strain increments. The total strain increment $d\epsilon_i$ is separated into elastic and plastic parts:

$$d\epsilon_i = d\epsilon_i{}^e + d\epsilon_i{}^p \quad (16)$$

As shown by Marcal,[2] $d\epsilon_i$ can be related to $d\sigma_i$ and $d\bar{\epsilon}_p$ as follows:

$$\begin{Bmatrix} d\epsilon_1 \\ d\epsilon_2 \\ 0 \end{Bmatrix} = \{K\} \begin{Bmatrix} d\sigma_1 \\ d\sigma_2 \\ d\bar{\epsilon}_p \end{Bmatrix} \quad (17)$$

and $\{K\}$ is a 3×3 stiffness matrix.

von Mises Yield Criterion

For the von Mises yield criterion,

$$\{K\} = \begin{bmatrix} 1/E & -\nu/E & S_1/\bar{\sigma} \\ -\nu/E & 1/E & S_2/\bar{\sigma} \\ S_1/\bar{\sigma} & S_2/\bar{\sigma} & -H' \end{bmatrix} \quad (18)$$

where $S_1 = \sigma_1 - \sigma_2/2$ and $S_2 = \sigma_2 - \sigma_1/2$. The quantity H' is the slope of the equivalent stress-equivalent plastic strain curve,

$$H' \equiv d\bar{\sigma}/d\bar{\epsilon}_p \quad (19)$$

where

$$\bar{\sigma} = (\sigma_1{}^2 - \sigma_1\sigma_2 + \sigma_2{}^2)^{1/2}$$

$$d\bar{\epsilon}_p = 2[(d\epsilon_1{}^2 + d\epsilon_1 d\epsilon_2 + d\epsilon_2{}^2)]^{1/2}/3^{\frac{1}{2}}$$

The elastic-plastic moduli E_{ij} found by taking the inverse of $\{K\}$ become

$$E_{11} = (H'\bar{\sigma}^2 + ES_2{}^2)/D \quad (20a)$$

$$E_{12} = (\nu H'\bar{\sigma} - ES_1S_2)/D \quad (20b)$$

$$E_{13} = (\nu S_2\bar{\sigma} + S_1\bar{\sigma})/D \quad (20c)$$

$$E_{21} = E_{12} \quad (20d)$$

$$E_{22} = (H'\bar{\sigma}^2 + ES_1{}^2)/D \quad (20e)$$

$$E_{23} = (S_2\bar{\sigma} + \nu S_1\bar{\sigma})/D \quad (20f)$$

$$E_{31} = E_{13} \quad (20g)$$

$$E_{32} = E_{23} \quad (20h)$$

$$E_{33} = -(1 - \nu^2)\bar{\sigma}^2/ED \quad (20i)$$

where

$$D = (1 - \nu^2)H'\bar{\sigma}^2/E + S_1{}^2 + 2\nu S_1S_2 + S_2{}^2$$

E = Young's modulus, ν = Poisson's ratio

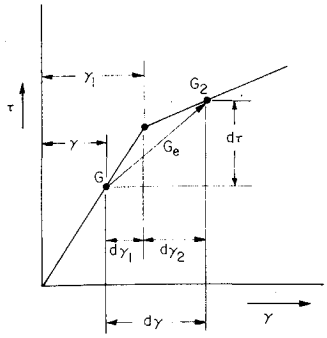

Fig. 1 Effective shear modulus for a transition region.

These values of E_{ij} agree with those found independently by Popov, Khojasteh-Bakht and Yaghmai.[14]

For the von Mises yield criteria the stiffnesses of Eq. (12) are evaluated by numerical integration using the above expressions for the elastic-plastic moduli E_{ij}. Following Marcal and Pilgrim,[2] stresses are stored at 11 points through the shell thickness and integration is performed with the trapezoidal rule.

Tresca Yield Criterion

For the Tresca yield criterion, the maximum shear stress τ_0 is used in place of $\bar{\sigma}$ and an associated plastic shear strain $d\gamma_p$ is used in place of $d\bar{\epsilon}_p$. The maximum shear stress can be either one of six quantities, depending upon which side of the Tresca yield surface governs yielding, i.e.,

$$f_k = 2\tau_0 \text{ for } f_k \geq f_i,\ i \neq k;\quad i,k = 1,2,\ldots,6 \tag{21}$$

where

$$\begin{aligned} f_1 &= \sigma_1 - \sigma_3,\ f_2 = -\sigma_1 + \sigma_3,\ f_3 = \sigma_2 - \sigma_3 \\ f_4 &= -\sigma_2 + \sigma_3,\ f_5 = \sigma_1 - \sigma_2,\ f_6 = \sigma_2 - \sigma_1 \end{aligned} \tag{22}$$

and where $\sigma_3 = 0$ for a plane stress state. The plastic strains are given by potential flow law

$$d\epsilon_i^p = \lambda \partial f_k / \partial \sigma_i \tag{23}$$

The associated plastic shear strain $d\gamma_p$ depends on f_k; for k equals 1–6, $d\gamma_p$ is, respectively, $d\epsilon_1^p - d\epsilon_3^p$; $-d\epsilon_1^p + d\epsilon_3^p$; $d\epsilon_2^p - d\epsilon_3^p$; $-d\epsilon_2^p + d\epsilon_3^p$; $d\epsilon_1^p - d\epsilon_2^p$; $-d\epsilon_1^p + d\epsilon_2^p$. It should be noted that $d\epsilon_3^p \neq 0$, even though $\sigma_3 = 0$ for a plane stress state.

For the Tresca criterion, H' is given by the slope of a shear stress vs plastic shear strain curve, i.e.,

$$H' \equiv d\tau_0 / d\gamma_p \tag{24}$$

The stiffness matrix $\{K\}$ differs for the various f_k:

$$K_{11} = K_{22} = 1/E \text{ for all } f_k \tag{25a}$$

$$K_{12} = K_{21} = -\nu/E \text{ for all } f_k \tag{25b}$$

$$K_{33} = -H' \text{ for all } f_k \tag{25c}$$

$$K_{13} = K_{31} = \pm\tfrac{1}{2} \text{ and } K_{23} = K_{32} = 0 \text{ for } f_{1,2} \tag{25d}$$

$$K_{13} = K_{31} = 0 \text{ and } K_{23} = K_{32} = \pm\tfrac{1}{2} \text{ for } f_{3,4} \tag{25e}$$

$$K_{13} = K_{31} = \pm\tfrac{1}{2} \text{ and } K_{23} = K_{32} = \mp\tfrac{1}{2} \text{ for } f_{5,6} \tag{25f}$$

By inversion of $\{K\}$, the E_{ij} are found. These again vary

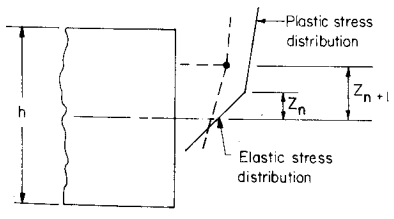

Fig. 2 Transition region within shell thickness.

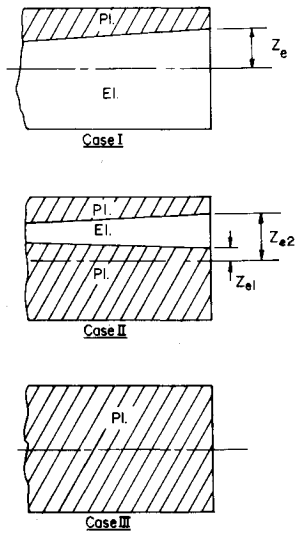

Fig. 3 Types of elastic-plastic zones for loading.

for the f_k

$$k = 1,2\ \ E_{11} = H'/D,\ E_{12} = \nu H'/D,\ E_{13} = \pm 1/2D \tag{26a}$$

$$E_{22} = (H' + E/4)/D,\ E_{23} = \pm\nu/2D \tag{26b}$$

$$E_{33} = -(1 - \nu^2)/ED \tag{26c}$$

$$D = H'(1 - \nu^2)/E + \tfrac{1}{4} \tag{26d}$$

$$k = 3,4\ E_{11} = (H' + E/4)/D,\ E_{12} = \nu H'/D \tag{27a}$$

$$E_{13} = \pm\nu/2D,\ E_{22} = H'/D \tag{27b}$$

$$E_{23} = \pm 1/2D,\ E_{33} = -(1 - \nu^2)/ED \tag{27c}$$

$$D = H'(1 - \nu^2)/E + \tfrac{1}{4} \tag{27d}$$

$$k = 5,6\ E_{11} = (2H' + E/2)/D \tag{28a}$$

$$E_{12} = (2\nu H' + E/2)/D,\ E_{13} = \pm(1 - \nu)/D \tag{28b}$$

$$E_{22} = (2H' + E/2)/D \tag{28c}$$

$$E_{23} = \mp(1 - \nu)/D,\ E_{33} = -2(1 - \nu^2)/ED \tag{28d}$$

$$D = 2H'(1 - \nu^2)/E + (1 - \nu) \tag{28e}$$

It is noted that if H' is constant then the E_{ij} are constant. If $H' = H'_n$ is constant for a purely plastic zone between z_n and z_{n+1} in a shell, then E_{ij}^n = constant, and if yielding is governed by only one f_k in this zone, then the contribution of the integrals in Eq. (12) between z_n and z_{n+1} are simply:

$$\Delta_n C_{ij} = E_{ij}^n (z_{n+1} - z_n) \tag{29a}$$

$$\Delta_n K_{ij} = E_{ij}^n (z_{n+1}^2 - z_n^2)/2 \tag{29b}$$

$$\Delta_n D_{ij} = E_{ij}^n (z_{n+1}^3 - z_n^3)/3 \tag{29c}$$

where

$$\Delta_n C_{ij} = \int_{z_n}^{z_{n+1}} E_{ij} dz, \text{ etc.}$$

However, for a transition from an elastic zone to a plastic zone during a load increment, the stiffnesses become more difficult to evaluate.

The procedure used here is similar to that used by Marcal,[2] who introduced a mean stiffness as follows:

$$E_{ij}|_{\text{mean}} = mE_{ij}|_{\text{elastic}} + (1 - m)E_{ij}|_{\text{el-pl}} \tag{30}$$

where $(\partial\sigma_i/\partial\epsilon_j) = E_{ij}$. The mean stiffness is a weighted average of the elastic stiffness and the elastic-plastic stiffness at the strain reached after the increment in load. Here m is a weighting factor, $0 \leq m \leq 1$.

A value for m is found here from consideration of the maximum shear stress-shear strain curve. With reference

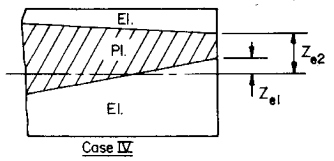

Fig. 4 Type of elastic-plastic zone when local unloading occurs with loading.

to Fig. 1, an effective shear modulus G_e is defined as follows:

$$d\gamma = d\gamma_1 + d\gamma_2 \tag{31a}$$

$$d\tau = Gd\gamma_1 + G_2 d\gamma_2 \equiv G_e d\gamma \tag{31b}$$

$$G_e = m(G - G_2) + G_2 \tag{31c}$$

$$m = d\gamma_1/d\gamma \tag{31d}$$

$$d\gamma_1 = \gamma_1 - \gamma \tag{31e}$$

where γ_1 is the yield value of the shear strain. It can be shown that $G_2 = H'/(1 + H'/G) \cdot d\gamma$ is the predicted shear strain increment for a load increment or it is the calculated shear strain increment after each iteration of the solution.

In a Kirchhoff shell, $d\epsilon_1$ and $d\epsilon_2$, and hence $d\epsilon_3$ and $d\gamma$ are linear functions of z. Therefore, the weighting factor m is a function of z as follows:

$$m = (az + b)/(cz + d) \tag{32}$$

where the coefficients a,b,c, and d are functions of $\gamma_1, \epsilon_\theta, \epsilon_\phi, \kappa_\theta, \kappa_\phi, d\epsilon_\theta, d\epsilon_\phi, d\kappa_\theta$, and $d\kappa_\phi$.

A transition region through the shell thickness is described in reference to Fig. 2. The elastic-plastic interface is assumed to be at z_{n+1} before the increment in load and is assumed to be at z_n after the load increment. Referring to Eq. (12), with the modified form of the stiffnesses Eq. (30), it is noted that the following integrals need to be evaluated:

$$\int m dz, \int mz dz, \int mz^2 dz \tag{33}$$

These integrals are easily evaluated. The resulting stiffnesses for the transition region are expressed as

$$\Delta_n C_{ij} = (E_{ij}{}^n - E_{ij}{}^{n+1}) I_1{}^n + E_{ij}{}^{n+1}(z_{n+1} - z_n) \tag{34a}$$

$$\Delta_n K_{ij} = (E_{ij}{}^n - E_{ij}{}^{n+1}) I_2{}^n + E_{ij}{}^{n+1}(z_{n+1}{}^2 - z_n{}^2)/2 \tag{34b}$$

$$\Delta_n D_{ij} = (E_{ij}{}^n - E_{ij}{}^{n+1}) I_3{}^n + E_{ij}{}^{n+1}(z_{n+1}{}^3 - z_n{}^3)/3 \tag{34c}$$

where $I_i{}^n$ are functions of z given in Appendix A.

The total shell stiffnesses can be found by adding the contributions from Eqs. (29) and (34) for elastic, transition, and plastic regions, $n = 1,2, \ldots, N$, i.e.,

$$C_{ij} = \sum_{n=1}^{N} \Delta_n C_{ij} \text{ etc.} \tag{35}$$

Types of Elastic-Plastic Zones

It is advantageous for computer storage requirements to minimize the number of regions N that need to be considered. This can be done by assuming a bilinear approximation to the stress strain curve ($\tau - \gamma$ curve). In this case, only four storage points (at most) are needed through the thickness and only six z coordinates are needed in the calculation of stiffnesses.

Three types of elastic-plastic zones are shown in Fig. 3. There is also the initial all-elastic zone which is not shown in the figure. Start of a plastic zone can be detected by checking the surface stresses and comparing with the yield limit.

Figure 4 shows the type of elastic-plastic zone that can occur when certain local unloading occurs during loading. Unloading occurs if the stresses become less than the yield

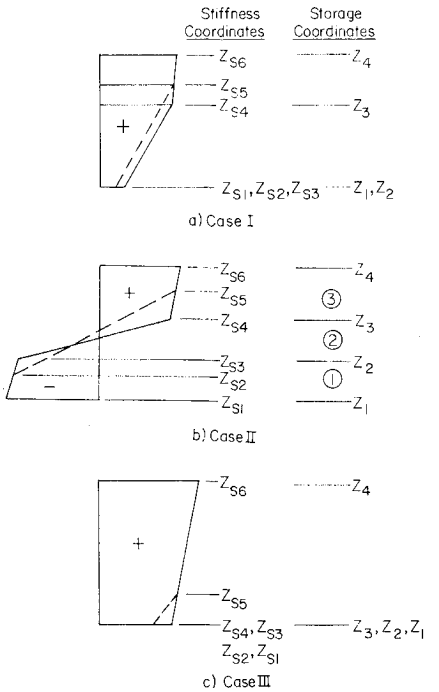

Fig. 5 Stress distributions and coordinates of elastic-plastic zone for loading.

values in an originally plastic region and can be checked by

$$\gamma d\gamma^p \geq 0 \text{ for loading} \tag{36}$$

If $d\gamma^p$ becomes equal to zero, unloading can occur.

For the assumed bilinear approximation, the coordinates and the stress distributions for the three loading zones and the unloading zone are shown in Figs. 5 and 6. The Case IV type zone from local unloading shown in Figs. 4 and 6 is not the only one. Different cases can also occur during unloading.

For a Case I type, the stiffnesses are particularly simple. For example,

$$C_{ij} = E_{ij}{}^2(z_{S4} - z_{S3}) + (E_{ij}{}^2 - E_{ij}{}^3) I_1{}^4 + E_{ij}{}^3(z_{S5} - z_{S4}) + E_{ij}{}^3(z_{S6} - z_{S5}) \tag{37}$$

In this case as in others, it is assumed that, for example, E_{ij} is constant between z_{S4} and z_{S6} (Fig. 5). This is true for linear strain hardening (H' = constant) and if the same Tresca yield function f_k governs at both z_{S4} and z_{S6}. If the same f_k does not govern at both of these points, another coordinate needs to be located intermediate in the plastic zone.

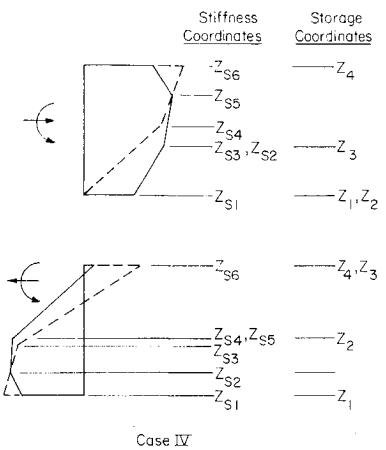

Fig. 6 Stress distributions and coordinates of elastic-plastic zones for local unloading with loading.

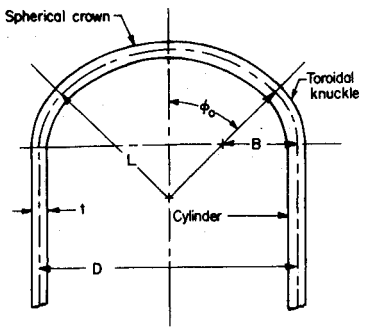

Fig. 7 Geometry of a torispherical-head pressure vessel.

Multisegment Numerical Integration Method

Numerical integration routines are available for most digital computers. The routines contain various methods of integrating systems of first order ordinary differential equations. These methods include Runge-Kutta, Runge-Kutta-Gill, Adams, Adams-Moulton, etc. All are based upon a Taylor's series expansion of the fundamental variables. Modifications are made to control accuracy.

The authors' computer program NONLEP (Nonlinear elastic-plastic analysis of shells) is an extension of an earlier program NONLIN for elastic analysis.[11] The numerical integration routine used in the program employs an Adams-Moulton scheme with Runge-Kutta-Gill as a starter. Errors are locally controlled at each integration step with automatic variation in step size as needed. The main advantage of numerical integration over the finite difference approach is that the iteration of mesh size required for the latter is eliminated.

In shell analysis another problem arises. Edge zones exist in the solutions near boundaries. The solutions are of exponential type and accuracy is lost in integrating over long path lengths. To overcome this problem the multisegment method of Kalnins and Lestingi[1,11] is used. This method provides uniform accuracy everywhere along the integration path (meridian of a shell).

The integration path length S is divided into a number of segments ΔS. ΔS should be chosen to be less than or equal to the "decay length" for an elastic shell, i.e.

$$\Delta S \leq 3(rh)^{1/2}$$

The nonlinear elastic-plastic boundary value problem is then solved by a double iteration procedure as follows:

1) A trial solution of Eqs. (1–6) is integrated from S_i to $S_i + \Delta S_i$ in every segment, and both the fundamental variables and the auxiliary variables appearing on the right side of Eqs. (1–6) are stored at the end of each segment. The trial solution may be a linear elastic solution at a first load step or an extrapolated nonlinear elastic-plastic solution from a prior load step.

In the elastic plastic range the load is incremented. Total strain increments $\Delta\epsilon$ are assumed for the next increment in load for the first trial solution at the new load. (Resulting $\Delta\epsilon$'s are used for further iterations of the solution.) Predicted values for $\Delta\epsilon_\phi, \Delta\epsilon_\theta, \Delta\kappa_\phi, \Delta\kappa_\theta$, and the elastic-plastic interface coordinates Z_e are calculated. By using these, new stiffnesses C_{ij}, K_{ij} and D_{ij} are calculated. The latter are used in the differential equations for each iteration of numerical integration. Each segment is divided into a number of storage points. Residual stress and strain values are stored from the previous load level, and current values are stored from each integration at the new load level.

2) Resulting strain increments $\Delta\epsilon_\phi, \Delta\epsilon_\theta, \Delta\kappa_\phi$ and $\Delta\kappa_\theta$ are determined and compared with predicted values. Step 1 is repeated until the resulting and predicted values agree. Usually two or three iterations on the strain increments (and the stiffnesses) are sufficient.

3) Using the method of Fox,[15] the changes in the fundamental variables due to changes in the initial conditions at the beginning of segments can also be expressed (from a first order Taylor series) in differential equation form. These equations are also integrated over each segment and the matrix of derivatives relating the changes are stored at the end of the segments. This integration is done simultaneously with step 1.

4) Newton's rule[15] is used to predict new initial values of the fundamental variables, and the integrations are repeated. Continuity of the fundamental variables between adjacent segments and the boundary conditions at the end of the path are checked. If continuity and the boundary conditions are satisfied within the desired accuracy then convergence has been obtained, otherwise the iteration procedure of steps 1–4 is repeated.

Numerical Results

The torispherical-head pressure vessel shown in Fig. 7 was analyzed for the parameters $\phi_0 = 30°$, $D/B = 16$ and $D/t = 200$. Young's modulus was taken as 30×10^6 psi, the material yield strength as 30,000 psi and the diameter as 200 in.

Figure 8 shows the inward deflection in the knuckle area at the coordinate $\phi = 50$ as a function of internal pressure. The separate curves indicate the effects of large deformation and strain hardening. A bilinear stress-strain curve was assumed with 10% strain hardening (slope in the plastic range of $\frac{1}{10}$ the elastic slope). The dashed curves were located on the basis of the two limiting materials, and indicate the effects of smaller amounts of strain hardening. Significant strengthening effects are evident due both to the favorable shape changes and strain hardening. All of the curves of Fig. 8 are for the von Mises yield criterion.

The pressures P_1 and P_2 indicated in Fig. 8 are limit pressures reported in the literature. Both are based on small deflection analysis. The pressure P_1 is the collapse pressure predicted by the limit analysis of Drucker and Shield[16] using the Tresca yield criterion. Crisp[17,18] using the method of Marcal and Pilgrim[2] reports the results of a parametric study of torispherical heads, and defines an excessive deformation pressure as that to produce a plastic strain of 1%. The pressure P_2 was determined in this manner, and is based on a small deflection analysis and the von Mises yield criterion. It is of interest to note that applying a factor of 1.15 brings P_1 into near agreement with P_2. The factor 1.15 is a scale factor between the von Mises and Tresca criteria.

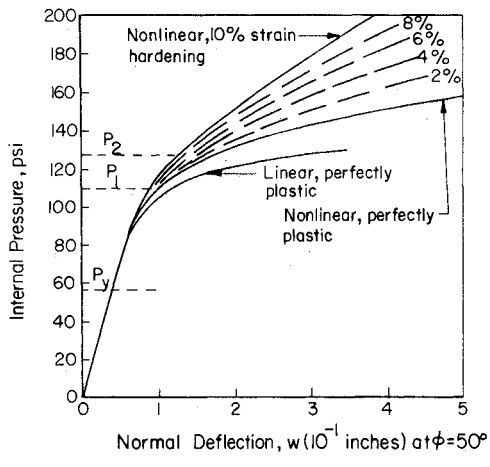

NOTE:
Cylinder collapse pressure, p = 347 psi.
P_1 = Limit analysis collapse pressure of Drucker & Shield.
P_2 = Excessive deformation pressure of CEGB analysis.

Fig. 8 Pressure vs deflection at location of initial yield, elastic-plastic analysis of torispherical-head pressure vessel, $D/t = 200$, $D/B = 16$, $\phi_0 = 30°$.

In pressure vessel design the allowable stress is often given in terms of a stress intensity index. The index ISI is defined as

$$\text{ISI} = \max\{|\sigma_{\phi_0}|, |\sigma_{\theta_0}|, |\sigma_{\phi i} + p|, |\sigma_{\theta i} + p|, |\sigma_{\phi_0} - \sigma_{\theta_0}|, |\sigma_{\phi i} - \sigma_{\theta i}|\}$$

and corresponds to an effective stress defined as twice the maximum shear stress. Using this index the stress distribution in the torispherical head is shown in Fig. 9. Results for both the von Mises and Tresca criteria are shown for a pressure beyond the initial yield pressure. The two criteria give results in virtual agreement, except for the plastic zone within the knuckle. Here ISI is limited for the Tresca criterion by the yield stress of 30,000 psi. The stress for the von Mises criterion exceeds this value, but by 15% or less in accord with the difference between the yield criteria.

Pressurized Expansion Bellows

The deflections in metallic bellows and diaphragms can become very large. Figure 10 shows a calculated pressure deflection curve for a 347 stainless steel formed bellows. Measured deflections as reported in Ref. 11 are also shown. For this bellows, the diameter and wall thickness were nominally 5 in. and 0.01 in., respectively. The bellows length was 4.14 in. and it had 12 convolutions. However, the analysis was based on actual cross section and variable thickness data as measured on a typical convolution of a similar bellows of the same manufactured lot. A bilinear approximation was used for the stress strain curve of the 347 annealed stainless steel sheet material. The yield strength was taken as 35,000 psi and the slope of the stress strain curve in the plastic range as 1.2×10^6 psi.

In the analysis, only one half a convolution was considered and symmetry boundary conditions were assumed. The loading was one of internal pressure. In addition, the ends of the bellows were assumed fixed so that no net axial deflection could occur.

Calculations were carried out up to pressures of 300 psi, whereas the initial yield pressure was found to be 68.8 psi. Deflections of several times the thickness are noted. The calculated curve is seen in Fig. 10 to lie somewhat above the experimental points, but provides a good envelope to the data points. The yield strength and strain hardening characteristics of the actual bellows material were not exactly known. It is believed that suitable adjustments in these parameters could bring the theory and experiment into much closer agreement. The geometry of the bellows could have had some circumferential variation which would affect the deflection behavior. In fact, the differences in deflection as measured on the right and left show this effect quite well. Also the experimental measurements made with a micrometer are sensitive to the exact point where they are measured, noted as approximately 0.18 in. in from the crown in Fig. 10. An asymmetrical mode of deformation became evident in the tests at pressures in the 250 psi range. This may explain

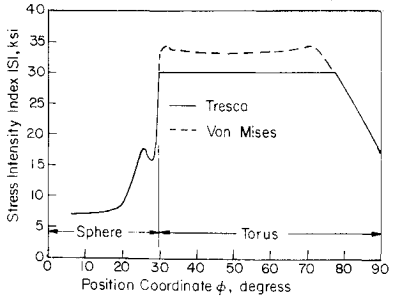

Fig. 9 Stress intensity index for torispherical-head with $D/t = 200$, $D/B = 16$, $\phi_o = 30°$, and pressure = 75.2 psi.

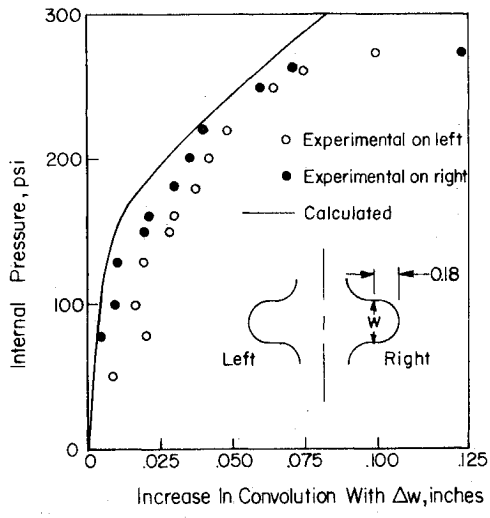

Fig. 10 Pressure deflection curve for expansion bellows.

the apparent asymptotic trend of the experimental points while the predicted curve continues to rise.

Appendix A

The integrals I_j^n in the stiffness equation (34) are evaluated here. The I_j^n are given in the following form

$$I_1^n = aJ_2 + bJ_1,\ I_2^n = aJ_3 + bJ_2,\ I_3^n = aJ_4 + bJ_3$$

where

$$J_1 = \int_{z_n}^{z_{n+1}} \frac{dz}{cz+d} = \left[\frac{\log(cz+d)}{c}\right]_{z_n}^{z_{n+1}}$$

$$J_2 = \int_{z_n}^{z_{n+1}} \frac{zdz}{cz+d} = \left[\frac{-d}{c^2}\log(cz+d) + \frac{z}{c}\right]_{z_n}^{z_{n+}}$$

$$J_3 = \int_{z_n}^{z_{n+1}} \frac{z^2dz}{cz+d} = \left[\frac{d^2}{c^3}\log(cz+d) + \frac{z^2}{2c} - \frac{zd}{c^2}\right]_{z_n}^{z_{n+}}$$

$$J_4 = \int_{z_n}^{z_{n+1}} \frac{z^3dz}{cz+d} = \left[\frac{-d^3}{c^4}\log(cz+d) + \frac{z^3}{3c} - \frac{d}{2c^2}z^2 + \frac{d^2}{c^3}z\right]_{z_n}^{z_{n+}}$$

References

[1] Kalnins, A. and Lestingi, J. F., "On Nonlinear Analysis of Elastic Shells of Revolution," *Transactions of the ASME, Ser. E: Journal of Applied Mechanics*, Vol. 34, March 1967, pp. 59–64.

[2] Marcal, P. V. and Pilgrim, W. R., "A Stiffness Method for Elastic-Plastic Shells of Revolution," *Journal of Strain Analysis*, Vol. I, No. 4, 1966, pp. 339–350.

[3] Marcal, P. V., "Large Deflection Analysis of Elastic-Plastic Shells of Revolution," AIAA/ASME 10th Structures, Structural Dynamics, and Materials Conference, New Orleans, April 14–16, 1969.

[4] Marcal, P. V., "Finite Element Analysis of Combined Problems of Non-linear Material and Geometrical Behavior," *Computational Approaches in Applied Mechanics*, ASME, 1970.

[5] Marcal, P. V., "Large Deflection Analysis of Elastic-Plastic Plates and Shells," *Proceedings of the First International Conference on Pressure Vessel Technology*, Part I, Design and Analysis, ASME, 1969, pp. 75–87.

[6] Yaghmai, S., "Incremental Analysis of Large Deformations in Mechanics of Solids with Applications to Axisymmetric Shells of Revolution," Rept. CR-1350, June 1969, NASA.

[7] Popov, E. P. and Yaghmai, S., "Linear and Nonlinear Static Analysis of Axisymmetric Loaded Thin Shells of Revolution," *Proceedings of the First International Conference on Pressure Vessel Technology*, Part I, Design and Analysis, ASME, 1969, pp. 237–244.